THE JOURNAL OF PHYSICAL CHEMISTRY C

Article

pubs.acs.org/JPCC

Theoretical Study of the Stoichiometric and Reduced Ce-Doped TiO_2 Anatase (001) Surfaces

Anderson R. Albuquerque,[†,‡,§] Albert Bruix,[§] Julio R. Sambrano,[‡] and Francesc Illas*[,§]

[†]Instituto Federal de Educação, Ciência e Tecnologia do Sertão Pernambucano, IF Sertão-PE, CEP, 56400-000 Floresta, PE Brazil

[‡]Grupo de Modelagem e Simulação Molecular, INCTMN-UNESP, São Paulo State University, CEP 17033-360, Bauru, SP Brazil

[§]Departament de Química Física & Institut de Química Teòrica i Computacional (IQTCUB), Universitat de Barcelona, C/Martí i Franquès 1, E-08028 Barcelona, Spain

ABSTRACT: The effects of Ce doping (2.6%) on the oxygen vacancy (V_O) formation energy (E_f) and the electronic structure of the anatase TiO_2(001) surface were studied by means of periodic density functional calculations within the PBE and PBE + U approaches. Several situations were considered for V_O formation, differing in terms of the position in relation to the dopant site (at the surface and subsurface atomic layers). The vacancy energy of formation is almost always lower for the surface than for the bulk, but the difference is still larger with Ce dopant in the subsurface layers. Nevertheless, the Ce-for-Ti substitution is more stable at the outermost layers, indicating thermodynamically favorable dopant migration toward the oxide surface. The PBE + U approach provides a physically meaningful description of localized d and f electrons in Ti^{3+} and Ce^{3+} species, respectively. Moreover, fully localized spin (simple and split) or partially localized spin solutions are found within a ~0.5 eV range. Not unexpectedly, standard PBE fails to describe electron-localized solutions, but interestingly, it predicts the same geometries and order of stability of different vacancy positions. The present work provides compelling evidence that oxygen vacancy formation is remarkably facilitated by Ce dopant in TiO_2 anatase {001} facets, but only when Ce is in subsurface positions.

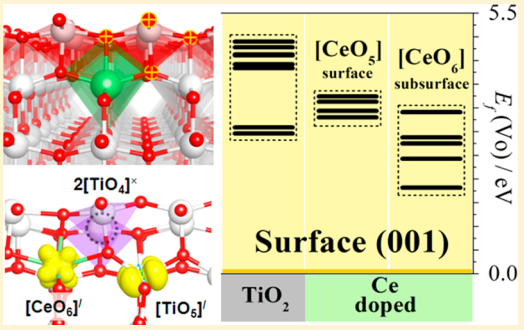

1. INTRODUCTION

Titanium dioxide (TiO_2) is one of the most studied metal oxides, partially because of its (photo)catalytic properties.[1−3] Among the different TiO_2 polymorphs, the anatase phase has always received the most attention because of its superior activity in comparison to the rutile and brookite phases.[4] However, the wide band gap (3.20−3.51 eV)[5,6] of TiO_2 anatase restricts its applicability as a photocatalyst to the ultraviolet range only. Many strategies have been suggested to improve the photocatalytic activity of TiO_2, such as introducing crystal disorder,[7] exposing highly reactive facets,[8] doping with metal and nonmetals,[9,10] creating point defects,[11] or mixing metal-oxide (MO_x/TiO_2) nanostructures.[12] Likewise, it is common to combine different strategies for designing new materials with improved catalytic properties. For example, the interaction between different metals (Pt, Cu, Au) and a CeO_x/TiO_2 mixed oxide support leads to very active catalysts for the water−gas shift reaction.[13,14]

The activity of catalysts containing CeO_2 or TiO_2 is largely due to their reducibility with a concomitant interplay between the number of Ce^{4+}/Ce^{3+} or Ti^{4+}/Ti^{3+} pairs and the formation of oxygen vacancies. In addition, the concentration of Ti^{3+} ($3d^1$) and Ce^{3+} ($4f^1$) centers in the reduced systems plays a fundamental role in their optical, chemical, and catalytic properties and can be modulated by adjusting the oxygen content.[10,15−19] Along this line, doping TiO_2 with Ce extends its photocatalytic activity to the visible region, which is directly attributable to the band-gap narrowing originating from the presence of Ce^{3+} ($4f^1$) states.[12,20−24] In a recent study, we investigated the effect of Ce doping (2.8−5.6%) on the reducibility of bulk TiO_2 anatase by means of calculations based on the density functional theory (DFT). We observed a significant decrease in the oxygen vacancy (V_O) formation energy, which is associated with a reduction of the Ce^{4+} cations to Ce^{3+} (instead of Ti^{4+} to Ti^{3+}) and to the distortion of the crystal structure.[25] A similar behavior was also described by means of theory and experiment by Johnston-Pack et al.[26] in mixed CeO_x/TiO_2 oxides, where the interface between the two oxides favors the formation and mobility of vacancies and Ce^{3+} centers. However, one must note that, as for any catalyst, the catalytic activity of ceria-anatase solid solutions is dominated by surface effects. Thus, whereas results regarding only the bulk provide precious information about the properties of anatase, a study involving surfaces is required to better assess the impact of Ce doping on its catalytic activity.

The importance of the surface is even greater when considering recent advances in the synthesis of nanometric metal-oxide single crystals that expose high-surface-energy

Received: October 20, 2014
Revised: January 12, 2015
Published: February 10, 2015

DOI: 10.1021/jp5105483
J. Phys. Chem. C 2015, 119, 4805−4816

facets[27] and sometimes exhibit superior catalytic activity.[28] The formation of these facets is usually partially inhibited during crystal growth under normal conditions, but it can be stabilized by reconstruction using capping agents or by interaction with other elements.[29,30] In the case of anatase, the lower surface energy of the (101) surface leads to particles/crystals that predominantly expose such termination. Nevertheless, facets exposing the less stable {001} termination have also been obtained, and it has been suggested that the catalytic properties of anatase crystals might arise from the lower stability (i.e., larger reactivity) of these facets.[27] In fact, it is possible to prepare either thin films that expose the less stable (001) surface[31] or anatase crystals exposing large percentages of {001} facets,[32,33] giving rise to the possibility of tailoring the activity of anatase crystals by modulating the ratio between the exposed areas for each different facet. In addition, the presence of surface and subsurface oxygen vacancies should also be taken into account because they significantly modify the reactivity and electronic properties of reduced TiO_2 surfaces and can even lead to severe surface reconstructions in extremely reducing conditions.[34]

In contrast to the large amount of work related to the (101) surface of anatase,[35−37] few studies have investigated the formation of oxygen vacancies and the properties of the localized holes and Ti 3d electrons at the (001) surface.[10,38,39] Based on DFT calculations, Ortega et al. reported more facile removal for oxygen atoms in the outermost oxygen layer of the (001) facet than those located in subsurface positions,[38] in agreement with previous results of Roldán et al. for Fe-doped anatase.[10] Using a more sophisticated hybrid DFT approach, Yamamoto and Ohno also studied the formation of vacancies and the nature of the trapped electrons and holes, attributing the origin of the optical absorption and luminescence in UV-irradiated anatase to such surface vacancies and to surface self-trapped holes.[39]

In the present work, we have investigated how the presence of the Ce dopant affects the reducibility of the Ce-doped TiO_2(001) surface and the electronic structure of the resulting systems. The influence of the Ce dopant on the reducibility and morphology of anatase TiO_2 was studied quite recently by Guo et al.,[40] although they focused on the interaction with sulfur-containing compounds such as tiophene. Here, instead, we provide a detailed description of the electronic states arising from the formation of oxygen vacancies in the Ce-doped anatase (001} surface. Thus, we have investigated the formation of vacancies at undoped and Ce-doped TiO_2(001), systematically considering various possibilities including surface and subsurface vacancies at different distances from the doping atoms and various electronic states differing in the position and localization of the trapped electrons generated upon O removal.

2. COMPUTATIONAL DETAILS

2.1. Structural Models. Periodic slab models were used to describe the stoichiometric and reduced Ce-doped TiO_2(001) anatase surfaces. The supercell used consisted of a 3 × 3 × 1 repetition of the conventional unit cell composed of 12 atoms: Ti_4O_8. This resulted in 36 TiO_2 units arranged in 12 atomic layers (or four O−Ti−O trilayers) in the z direction, where a ∼10 Å-wide vacuum region was included to minimize the interaction between repeated slabs. We expect that the reported dependence on slab thickness of the absolute values of vacancy formation energies in TiO_2-based systems due to relaxation and confinement effects[41] will affect Ce-doped and undoped systems to similar extents. Thus, the thickness of these slabs is considered to be sufficiently large to properly describe the effect of Ce doping on the vacancy formation energies of anatase (001). The (001) termination of anatase is known to undergo a (1 × 4) reconstruction when annealed at low oxygen pressures (under ultrahigh-vacuum conditions).[42,43] However, the unreconstructed structure can be recovered by exposing the surface to oxygen.[42] In addition, one should take into account that the creation of oxygen vacancies in the unreconstructed surface would be the first step before surface reconstruction under low O_2 pressure, which would require the removal of a larger number of O atoms. Thus, the unreconstructed (001) termination is a good model for describing the reduction of stoichiometric TiO_2(001). The slab models were constructed using the lattice parameters optimized at the Perdew−Burke−Ernzerhof (PBE) level reported in our previous study.[25] Upon generating vacancies or doping with Ce, further complete structural relaxation was taken into account but maintaining the lattice parameters of the stoichiometric system, which is a reasonable choice considering the small defect concentration of the systems under study. Ce-doped anatase (001) was studied by substituting one Ti atom with one Ce in the 108-atom surface supercell, resulting in a $Ti_{0.972}Ce_{0.028}O_2$ stoichiometry (2.8% Ce), well within the dopant concentration range preserving the Ce solid solution in anatase, because separation into anatase and CeO_2 fluorite phases occurs for Ce concentrations larger than 10%.[12]

Before describing the different structural possibilities of Ce-doped anatase, recall that, under vacuum conditions, the outermost layers of the (001) anatase surface consist of parallel five-fold-coordinated [TiO_5] polyhedra sharing oxygen atoms with two-fold ($O_{(2c)}$) and three-fold ($O_{(3c)}$) coordination in the x [10] and y [01] directions, respectively. Bulk-like [TiO_6] octahedra are found in subsurface positions, where all oxygen atoms have $O_{(3c)}$ coordination. Hence, two possibilities for Ce-for-Ti substitutions exist: one consisting of the substitution of an outermost Ti^{4+} cation, $[TiO_5]^{\times}$ + Ce → $[CeO_5]^{\times}$ + Ti (Figure 1a), and one resulting from a subsurface substitution, $[TiO_6]^{\times}$ + Ce → $[CeO_6]^{\times}$ + Ti (Figure 1b). In both cases, Ce acquires the oxidation state of the removed Ti^{4+} cation, and consequently, the substitution does not lead to the presence of unpaired electrons. The resulting electronic structure can thus be and has been studied without considering spin polarization.

The effect of Ce doping on the reducibility and electronic structure of the (001) surface of anatase was investigated by studying the formation of oxygen vacancies (V_O) on the TiO_2 and $Ti_{x-1}Ce_xO_2$ slab models just described. Removing one O atom from these slab systems results in $TiO_{1.986}$ (1.4% V_O) and $Ti_{0.972}Ce_{0.028}O_{1.986}$ (2.8% Ce and 1.4% V_O) stoichiometries. For the doped systems with the Ce atom either at the surface or in a subsurface layer, four different vacancy positions around the Ce^{4+} cation were considered, namely, V_{O1}, V_{O2}, V_{O3}, and V_{O4} in Figure 1. For the undoped system, oxygen atoms at three different positions were considered for vacancy formation; these positions are equivalent to V_{O1} ($O_{(2c)}$), V_{O2} ($O_{(3c)}$), and V_{O3} ($O_{(3c)}$) of Figure 1a but without the dopant. According to different DFT-based studies, the V_{O1} ($O_{(2c)}$) position is the most favorable position for oxygen vacancy formation in the stoichiometric anatase TiO_2(001) surface.[10,38,39] Nevertheless, to compare similar configurations on Ce-doped systems and bulk anatase, the other vacancy positions were also investigated. The situations considered lead to the reduction of different polyhedra. For the system with Ce dopant at the surface

DOI: 10.1021/jp5105483
J. Phys. Chem. C 2015, 119, 4805−4816

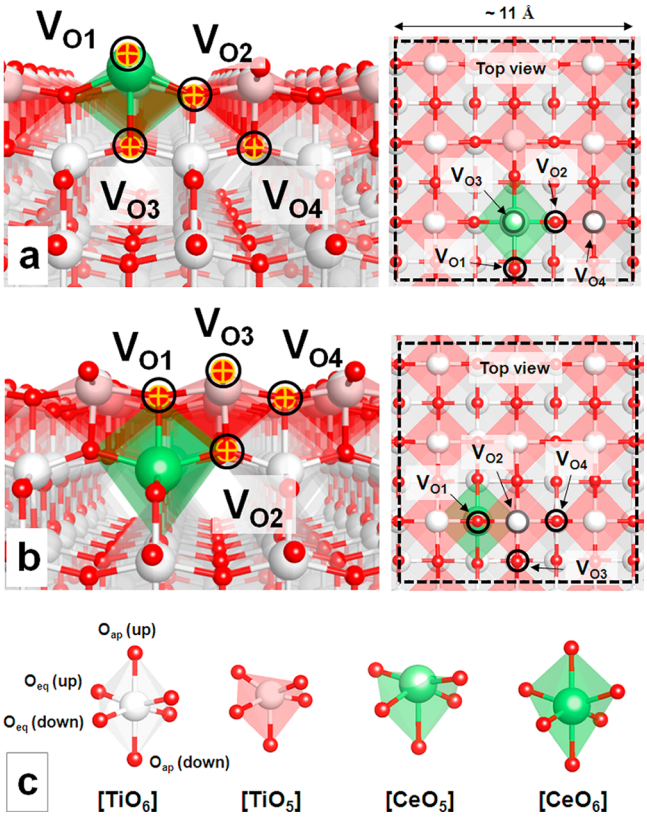

Figure 1. (Left) Side and (right) top views of the TiO_2 anatase (001) surface doped with one Ce atom substituting one Ti^{4+} cation in (a) a $[TiO_5]$ site of the outermost surface layer or (b) a $[TiO_6]$ site in the first subsurface layer. In each case, the different positions considered for removal of one oxygen atoms are indicated (V_{O1}–V_{O4}). (c) Different polyhedra present in these systems and their color codes: $[TiO_6]$, gray; $[TiO_5]$, red; and $[CeO_x]$, green. Red, gray, and green spheres represent oxygen, titanium, and cerium atoms, respectively.

(Figure 1a), three of the generated vacancies (V_{O1}–V_{O3}) lead to reduction on the $[CeO_5]$ polyhedra, whereas V_{O4} reduces the neighboring $[TiO_5][TiO_6]_2$. In addition, reduction at these positions can also lead in some cases to low-coordinated $[CeO_4]$ and $[TiO_4]$ distorted tetrahedral, as will be shown in the following. For the system with the Ce dopant in a subsurface position (Figure 1b), two V_O possibilities (V_{O1} and V_{O2}) result in the reduction of the $[CeO_6]$ octahedra, whereas for V_{O3} and V_{O4}, O atoms from neighboring Ti polyhedra are removed. Furthermore, the removal of a neutral O atom leaves two electrons in the system, giving rise to different electronic states depending on the degree of localization and spin coupling. The different states follow the description introduced in previous studies[25,44] and can generally be classified as (i) simply localized (or trapped) solution, where the two electrons are localized in atoms near the vacancy; (ii) split localized solution, where the two electrons are localized in next-nearest positions with respect to the O vacancy; (iii) the partially localized solution, where only one of the two electrons is localized and the other is delocalized; and (iv) fully delocalized solution, where the two electrons are delocalized around the unit cell. In addition to the possibility to localize one electron on a Ti^{4+} site leading to Ti^{3+}, one of the electrons can localize on the Ce site, triggering reduction from Ce^{4+} to Ce^{3+}. Note also that spin coupling can lead to a local open-shell singlet in the unit cell or to a local triplet state.

Because the bulk and slab supercell have the same composition ($Ti_{36-x}Ce_xO_{72-y}$), the (001) surface energy, E_{surf}, can be calculated directly as

$$E_{surf} = \frac{1}{2A}[E_{slab}(Ti_{36-x}Ce_xO_{72}) - E_{bulk}(Ti_{36-x}Ce_xO_{72})] \quad (1)$$

where A, $E_{slab}(Ti_{36-x}Ce_xO_{72})$, and $E_{bulk}(Ti_{36-x}Ce_xO_{72})$ correspond to the surface area of the slab, the total energy of the slab, and the energy of the $(3 \times 3 \times 1)$ unit cell of the bulk, respectively. For the doped systems, we calculated the substitution energy E_{dop} as

$$E_{dop} = [E_{slab}(Ti_{36-x}Ce_xO_{72}) - E_{slab}(Ti_{36}O_{72})] + x[E_{bulk}(TiO_2) - E_{bulk}(CeO_2)] \quad (2)$$

where $E(TiO_2)$ and $E(CeO_2)$ correspond to the calculated energies of bulk anatase and bulk CeO_2, respectively. The oxygen vacancy (V_O) formation energy, $E_f(V_O)$, was calculated as

$$E_f(V_O) = [E_{slab}(Ti_{36-x}Ce_xO_{72-y}) + y/2E(O_2)] - E_{slab}(Ti_{36-x}Ce_xO_{72}) \quad (3)$$

where $E(Ti_{36-x}Ce_xO_{72-y})$ corresponds to the energy of the (3×3) slab with x Ce atoms substituting x Ti atoms and y O atoms removed. For the undoped and doped surfaces, $x = 0$ and $x = 1$, respectively, and for the completely oxidized and partially reduced systems, $y = 0$ and $y = 1$, respectively. $E(O_2)$ is the energy of an isolated oxygen molecule in its ground triplet state.

2.2. Electronic Structure and Total Energy Calculations. Periodic DFT electronic structure calculations were carried out using the Vienna Ab Initio Simulation Package (VASP)[45,46] and the Perdew–Burke–Ernzerhof (PBE) semilocal form of the exchange–correlation functional within the generalized gradient approximation (GGA).[47] The Ti ($3p^64s^23d^2$), O ($2s^22p^2$), and Ce ($5s^25p^66s^24f^15d^1$) electrons were treated explicitly as valence electrons and were expanded in a plane-wave basis set including functions with a kinetic energy up to a cutoff value of 500 eV. The projector augmented wave (PAW) method was used to describe the interaction between the valence electrons and the (frozen) core electrons.[48] Two sets of calculations were performed: one using the standard PBE functional and one including an on-site Coulombic Hubbard-like U term to partially correct the electronic self-interaction error present in standard GGA functionals, leading to the so-called PBE + U approach (or, more generally, the DFT + U approach).[49] The rotationally invariant version of this approach by Liechtenstein and coworkers[50] was employed within the simplified spherically averaged version of Dudarev et al.,[51] where the effective interaction parameter ($U_{eff} = U - J$) was used instead of individual U and J terms. This method allows the description of the strongly correlated character of the Ti 3d and Ce 4f states found in reduced cerium and titanium oxides to be improved and has been successfully employed to describe reduced TiO_2[39] and CeO_2,[14,52] as well Ce-doped anatase[25,40] and the CeO_x/TiO_2[26] interface. The U parameter is usually determined so as to reproduce experimental data. Following previous work,[25] we applied the same value of 4 eV to correct both the Ti 3d and Ce 4f states, which is usually referred to as the PBE + U(4,4) approach. This pragmatic approach has a semiempirical flavor, but regarding the trends for vacancy formation energies in Ce-

DOI: 10.1021/jp5105483
J. Phys. Chem. C 2015, 119, 4805–4816

doped anatase and electronic structure feature (gap states), it has been shown to lead to results similar to those obtained with the more sophisticated, but still semiempirical, hybrid functional approach. It should be noted that GGA functionals are known to overbind the O_2 molecule. In our calculations, the uncorrected PBE approach was found to give a binding energy of −6.65 eV, which is significantly larger in magnitude than the −5.23 eV determined experimentally.[53] The partial correction of the self-interaction error through the addition of the U(O 2p) term provided an improved binding energy value of −5.74 eV. We therefore considered that the overbinding was sufficiently corrected by the addition of the on-site Coulomb interaction on the O 2p states. However, it is important to point out that the present study focused on the relative stability of different oxygen vacancies at surfaces, which were calculated using the same $E(O_2)$ value and were therefore not affected by the binding energy of the O_2 molecule.

For both the PBE and PBE + U approaches, spin polarization was taken into account in the calculations involving vacancies. The electronic solutions might vary depending on the character of the electrons left on the lattice upon O removal as described above (fully localized, partially localized, and delocalized) and the spin states. The open-shell triplet T_1 (ferromagnetic periodic solution) and broken-symmetry approximation to the open-shell singlet S_0 (antiferromagnetic periodic solution) were investigated when needed, first without any restriction and then biasing the calculation toward the desired solution with an appropriate initial guess. For the geometry optimization calculations, the reciprocal space was sampled using the Γ point only, but densities of states were calculated using a denser 5 × 5 × 1 mesh. The wave functions were self-consistently converged until differences in energy were lower than 10^{-4} eV, and the atomic positions of all atoms were fully relaxed until the largest component of the ionic forces was lower than 1×10^{-2} eV/Å.

3. RESULTS AND DISCUSSION

3.1. Stoichiometric and Ce-Doped Anatase. The atomic positions of stoichiometric and Ce-doped anatase TiO_2(001) surfaces were fully relaxed at the PBE and PBE + U levels. In both cases, the lattice parameters used to construct the supercell corresponded to those optimized at the PBE level ($a = b = 3.81$ Å and $c = 9.73$ Å), which are in close agreement with the experimental values of $a = b = 3.78$ Å and $c = 9.51$ Å.[54] The structural parameters of the [MO_6] and [MO_5] polyhedra (M = Ti or Ce) at the outermost surface and subsurface layers of the (001) surface are reported in Table 1. Substituting a Ce atom for a Ti atom (2.8% Ce concentration) leads to a structural deformation consisting of the expansion of the [CeO_x] polyhedra. The same behavior was also recently reported for bulk anatase,[25] where a volume expansion of around 30% with respect to [TiO_6] was found for [CeO_6], with the two apical Ce−O bonds experiencing a larger variation than the four equatorial bonds. On the (001) surface, the symmetry of the [MO_6] octahedra in the subsurface layer (C_{2v}) is different from the symmetry of the [MO_6] octahedra in the bulk (D_{2d}) because of the varying M−O bond lengths at different depths with respect to the surface. At both the PBE and PBE + U levels, the outermost M−O bonds are longer than the internal ones because of the greater flexibility of the outermost layer to accommodate to polyhedral expansion.

The surface energies (E_{surf}) for stoichiometric and Ce-doped anatase (001) surface were calculated in accordance with eq 1.

Table 1. Optimized Structural Parameters[a] of Stoichiometric and Ce-Doped Anatase TiO_2(001) Surfaces, with Bulk Values Included for Comparison

	undoped TiO_2		Ce-doped [a]	
structural parameter	PBE	PBE(4,4)	PBE	PBE(4,4)
(001) Surface: [MO_5] Polyhedra				
M−O (apical, down)	1.948	1.994	2.400	2.433
M−$O_{(2c)}$ (equatorial)	1.962	1.973	2.257	2.227
M−$O_{(3c)}$ (equatorial)	1.940	1.949	2.114	2.138
V [MO_5] (Å^3)	5.86	6.07	8.02	8.08
(001) Surface: [MO_6] Polyhedra				
M−O (apical, up)	1.989	2.024	2.261	2.325
M−O (apical, down)	2.013	2.041	2.249	2.296
M−O (equatorial, up)	1.949	1.956	2.168	2.146
M−O (equatorial, down)	1.952	1.958	2.137	2.135
V [MO_6] (Å^3)	9.66	9.82	12.79	12.81
Bulk: [MO_6] Only				
M−O (apical)	2.014	2.019	2.254	2.273
M−O (equatorial)	1.949	1.948	2.134	2.119
V [MO_6] (Å^3)	9.73	9.75	12.74	12.65

[a]Metal− (M = Ti, Ce) oxygen bond lengths in [MO_6] and [MO_5] polyhedra, and octahedron volume V at the PBE and PBE(4,4) levels.

The results for the PBE and PBE(4,4) levels of theory are reported in Table 2. The resulting E_{surf} values (~1.0 J.m^{-2}) do not vary significantly upon addition of the +U correction, in line with previous theoretical reports.[40,55,56] The presence of the Ce dopant in the subsurface layer does not significantly affect the surface energy. This is at variance with the situation in which the dopant Ce atom is located in the outermost [CeO_5] surface site, where the surface energy is reduced by 0.13−0.16 eV. This result is in agreement with previous work[25,40] and has been related to the greater abundance of exposed {001} facets in Ce-doped anatase, which follows from the Wulff construction relating lower surface energies to more abundant facets.[57,58] The increased stability of anatase (001) resulting from the presence of Ce dopants at the outermost surface layer also results in negative doping energies E_{dop} (ranging from −0.60 to −0.22 eV), in contrast with the positive values calculated for substitutions in the bulk (ranging from +1.51 to +2.46 eV) and in a subsurface [TiO_6] octahedron (ranging from +1.41 to +1.84 eV). This indicates that the formation of the solid solution at the (001) surface is stable and that dopant Ce atoms will be located predominantly at the anatase surface. Such a difference is not surprising because, whereas the low stability of this surface is reduced when its outermost region is distorted, the effect is not as large for bulk-like positions. This result also indicates that the migration of the doping Ce atoms from internal (bulk-like) positions to the outermost layers of the surface is thermodynamically favorable, which could lead to oxide phase segregation for sufficiently large Ce concentrations.

The density of states (DOS) of the anatase TiO_2(001) surface is qualitatively the same as that of the bulk[25] for both the PBE and PBE(4,4) levels of theory. The higher energy levels of the valence band (VB) correspond to O 2p states, and the lower energy levels of the conduction band (CB) correspond mainly to Ti 3d or Ce 4f states (Figure 2a). However, quantitative differences exist between the bulk and TiO_2(001) surface DOS, with the latter having a lower band gap. Nevertheless, one must note that the PBE exchange-correlation functional underestimates the band gap, although this is partially corrected at the PBE + U level (Table 2). The

DOI: 10.1021/jp5105483
J. Phys. Chem. C 2015, 119, 4805−4816

Table 2. Absolute Values of the Ce-Doping Energy (E_{dop}), Surface Energy (E_{surf}), and Band-Gap Energy (E_{gap}) of Bulk Anatase and the (001) Surface of Anatase, in Comparison with the Experimental Band Gaps

	E_{dop} (eV)		E_{surf} (J m^{-2})		E_{gap} (eV)		
system	PBE	PBE(4,4)	PBE	PBE(4,4)	PBE	PBE(4,4)	expt
TiO_2 bulk[25]	–	–	–	–	2.12	2.69	3.23[20]
$Ti_{1-x}Ce_xO_2$ bulk[25]	+1.51	+2.46	–	–	2.14	2.71	2.98[20]
TiO_2 surface (001)	–	–	1.03	1.05	1.56	2.14	–
$[CeO_5]$ surface (001)	−0.60	−0.22	0.90	0.89	1.17	1.67	–
$[CeO_6]$ subsurface (001)	+1.41	+1.84	1.02	1.01	1.54	2.09	–

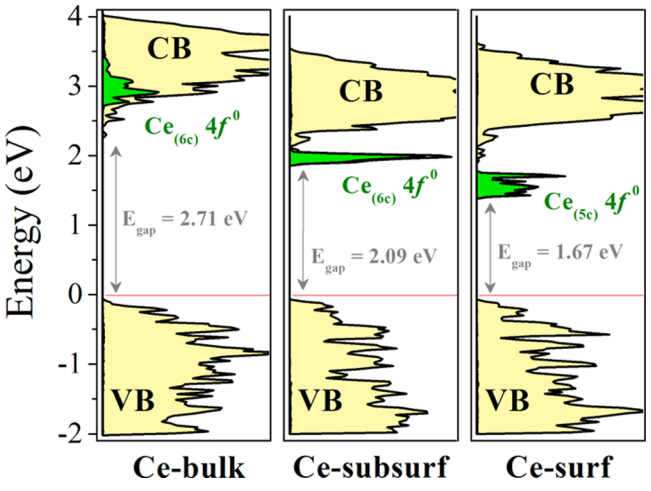

Figure 2. Density of states (DOS) of Ce-doped bulk and anatase TiO_2(001) surface at the PBE(4,4) level. The projected DOS for the dopants are shown in green. The top of VB was aligned to the Fermi level (red line) in each case.

latter leads to values in better agreement with (albeit still lower than) experiment (3.2 and 3.4 eV).[59] To fully reproduce the experimentally determined band gap, one should use U values larger than that used in the present work (4 eV), but this would also lead to excessively deep Ti^{3+} states in reduced titania.[60−62] Therefore, a compromise value was used here that provides reasonably accurate descriptions of the electronic structures of both stoichiometric and reduced anatase. The PBE(4,4)-calculated DOS also revealed other interesting differences between the surface and bulk of Ce-doped anatase. The position of the Ce 4f band was gradually lowered as the Ce dopant became closer to the surface, where it was found to be completely overlapping, just below, or well below the Ti 3d states for Ce at bulk, subsurface, or surface sites, respectively (Figure 2). This shift of the Ce 4f band toward lower energies was also found to lead to a ∼1 eV reduction of the band gap. A similar scenario was found for Ce dispersed in zirconia (ZrO_2), another 3d metal oxide, for which the photocatalytic activity was attributed to the presence of empty Ce 4f levels at the midgap of ZrO_2.[63]

The decrease in band gap of anatase upon doping, even with a low amount of Ce as reported by Watanabe et al.,[12] can be attributed to empty midgap Ce 4f states due to the presence of Ce at the (001) surface layers. However, this is not sufficient to explain the shoulders found in UV−visible and photoluminescence spectra, which suggests that there are also occupied Ce 4f states in the band gap corresponding to the presence of reduced Ce^{3+} cations. Therefore, to interpret the origin of the observed band-gap reduction, one must also consider the formation of oxygen vacancies at the oxide surface. This will be consistent with results reported for Ce-doped anatase where oxygen vacancies were found to lead to the partial occupation Ce 4f and Ti 3d levels.[25]

3.2. Oxygen Vacancies in Anatase TiO_2(001). Oxygen vacancies (V_O) are the most thermodynamically favored point defect in TiO_2 upon mild thermal treatment and under an oxygen-poor atmosphere. These point defects are more likely to occur for soft synthesis methods and are generally involved in the catalytic activity of TiO_2 through O-atom release or uptake in redox reactions.[64,65] These processes involve the migration of V_O (or O atoms) from the bulk to the surface (or vice versa). Herein, we report a systematic study of V_O formation at the anatase TiO_2(001) surface, focusing on the description of the trapped electrons formed upon the reduction of Ti^{4+} ($3d^0$) to Ti^{3+} ($3d^1$).

Table 3 summarizes the results obtained upon V_O generation on different anatase-based systems. Specifically, the spin coupling of the trapped electrons and the resulting V_O formation energy $E_f(V_O)$ are given for the stoichiometric and Ce-doped $TiO_{1.986}$(001) surface at both the PBE and PBE(4,4) levels. Results for the bulk systems with the same stoichiometry are included for comparison. The differences between vacancies at bulk and surface positions arise from the presence of undercoordinated $[TiO_5]$ polyhedra located at the outermost

Table 3. Calculated Oxygen-Vacancy Formation Energies (in eV) for Anatase Bulk and (001) Surface, Undoped and Ce-Doped as Predicted by the PBE and PBE(4,4) Levels of Theory[a]

system	V_O configuration	PBE	PBE(4,4)
bulk[25] TiO_2	V_O (singlet, S_0)	**3.68**−3.72	**4.82**−5.22
	V_O (triplet, T_1)	**3.91**−3.95	**4.90**−5.24
bulk[25] $Ti_{1-x}Ce_xO_2$	V_{O1}−V_{O4}	**3.11**−4.12	**3.74**−4.91
surface (001) TiO_2	V_{O1}	**1.29**$^{(s)}$, **1.49**$^{(t)}$	**2.66**$^{(s,t)}$, **2.96**$^{(t)}$, **3.09**$^{(s,t)}$
	V_{O2}	3.81$^{(s)}$, 3.98$^{(t)}$	4.34$^{(s)}$, 4.42$^{(t)}$, 4.63$^{(t)}$, 4.90$^{(s,t)}$
	V_{O3}	4.39$^{(s)}$, 4.40$^{(t)}$	4.61$^{(s,t)}$, 4.78$^{(t)}$
surface (001) $Ti_{1-x}Ce_xO_2$ Ce-doped $[CeO_5]$	V_{O1}	**2.21**$^{(t)}$	**3.30**$^{(t)}$
	V_{O2}	3.82$^{(t)}$	3.44$^{(s)}$
	V_{O3}	3.79$^{(t)}$	3.74$^{(t)}$
	V_{O4}	3.77$^{(t)}$	3.63$^{(t)}$
subsurface (001) $Ti_{1-x}Ce_xO_2$ Ce-doped $[CeO_6]$	V_{O1}	3.68$^{(t)}$	3.41$^{(t)}$
	V_{O2}	→ V_{O4}	→ V_{O4}
	V_{O3}	**0.35**$^{(s)}$, **0.68**$^{(t)}$	**1.82**$^{(t)}$, **2.43**$^{(t)}$
	V_{O4}	3.19$^{(t)}$	2.75$^{(s)}$, 2.88$^{(t)}$

[a]Most stable states for each level of theory considered are highlighted in bold (s, singlet; t, triplet).

DOI: 10.1021/jp5105483
J. Phys. Chem. C 2015, 119, 4805−4816

layers of the surface, which lead to more facile oxygen removal. The resulting Kröger–Wink notation for the formation of oxygen vacancies at different positions can be written as

$$V_{O1}:\quad [TiO_5]_m + [TiO_6]_n \rightarrow [TiO_5]_{m-2} + [TiO_6]_n + [TiO_4]_2 + V_{O1} + 2e + \frac{1}{2}O_2$$

$$V_{O2}:\quad [TiO_5]_m + [TiO_6]_n \rightarrow [TiO_5]_{m-2} + [TiO_6]_{n-1} + [TiO_4]_2 + [TiO_5] + V_{O2} + 2e + \frac{1}{2}O_2$$

$$V_{O3}:\quad [TiO_5]_m + [TiO_6]_n \rightarrow [TiO_5]_{m-1} + [TiO_6]_{n-2} + [TiO_4] + [TiO_5]_2 + V_{O3} + 2e + \frac{1}{2}O_2$$

$$\text{Bulk}:\quad [TiO_6]_n \rightarrow [TiO_6]_{n-2} + [TiO_5]_2 + V_O + 2e + \frac{1}{2}O_2$$

where $[TiO_5]$, $[TiO_6]$, and $[TiO_4]$ correspond to an outermost polyhedron or reduced bulk-like polyhedron, to the bulk-like octahedron, and to a reduced surface tetrahedron, respectively.

The calculated $E_f(V_O)$ values for bulk anatase are within the ranges 3.68–3.95 and 4.82–5.24 at the PBE and PBE(4,4) levels of theory, respectively. The corresponding values at the surface are significantly lower, ranging from 1.29 to 4.40 eV at the PBE level and from 2.66 to 4.90 eV at the PBE(4,4) level (Table 3). For both levels of theory, formation of V_{O1} by removal of an O atom from an $O_{(2c)}$ position results in the most stable oxygen vacancy in the anatase (001) surface, in agreement with previous work.[10,38] As was found for vacancies in the bulk, calculations with the uncorrected PBE functional resulted in states with electronic structures in which the two electrons left behind by the removed O atoms were delocalized through the whole lattice. In contrast, when the $+U$ correction was included, different electronic states with properly localized electrons were found; some are depicted in Figure 3. Even when the PBE spin density was completely delocalized, antiferromagnetic and ferromagnetic solutions were found for V_{O1}, V_{O2}, and V_{O3}, with the antiferromagnetic solutions generally being more stable (from 0.02 to 0.20 eV) than the ferromagnetic ones. Larger differences emerged when the $+U$ correction was included, where the two localized electrons could be located at several positions around the vacancy and with different spin couplings.

For the most stable vacancy position (V_{O1}), the configuration with both localized electrons in the $[TiO_4]$ tetrahedron around the vacancy was found, in agreement with previous reports.[39] The most stable electronic configuration corresponds to a localized solution (Figure 3a) in which unpaired electrons are found reducing two exposed $[TiO_4]^{/}$ polyhedra with E_f = 2.66 eV, in both singlet and triplet states. A second more stable configuration consists of a split localized solution formed by one exposed $[TiO_4]^{/}$ polyhedron and a subsurface $[TiO_5]^{/}$ polyhedron, with E_f = 2.96 eV. The third most stable V_{O1} is a partially localized solution, either an open-shell singlet or an open-shell triplet in the unit cell, with E_f = 3.09 eV, in which one electron is trapped on the $[TiO_4]^{/}$ tetrahedron whereas the other is delocalized over all other $[TiO_x]$ polyhedra. The generation of V_{O2} by removing one oxygen at $O_{(3c)}$ leads to four different configurations at the PBE(4,4) level with E_f values ranging from 4.34 to 4.90 eV. The most stable configuration (E_f = 4.34 eV) is a split solution with one reduced $[TiO_4]^{/}$ tetrahedron and one $[TiO_6]^{/}$ octahedron far in the subsurface (Figure 3b). This state is followed closely in terms of stability by a split solution with one reduced $[TiO_4]^{/}$ tetrahedron close to a $[TiO_6]^{/}$ octahedron (E_f = 4.42 eV) and by a simply localized solution (E_f = 4.63 eV) with $[TiO_4]^{/}$ + $[TiO_5]^{/}$ polyhedra around V_{O2}. Another much less stable solution for V_{O2} with E_f = 4.90 eV consists of a partially localized solution in which one electron is trapped on the subsurface $[TiO_6]^{/}$ polyhedron whereas the other is fully delocalized over the lattice.

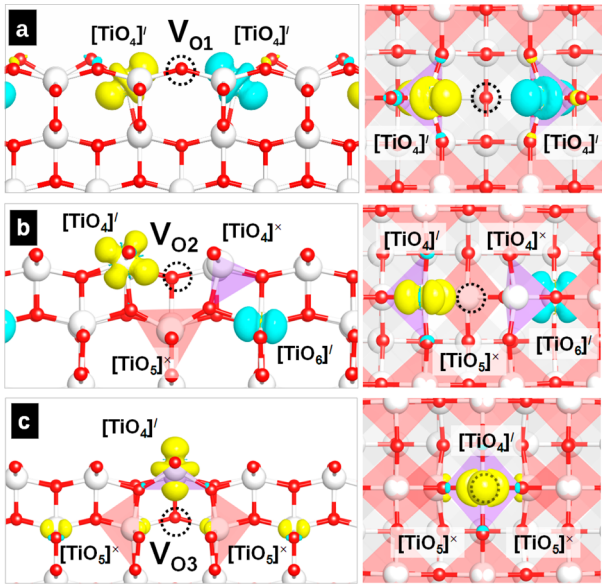

Figure 3. (Left) Side and (right) top views of the structure and spin density isosurfaces of the most stable configurations of reduced anatase TiO_2(001) at the PBE(4,4) level with V_O at different positions: (a) V_{O1} implies removing O from the $O_{(2c)}$ position, (b) V_{O2} removing O from $O_{(3c)}$ site at the outermost layer, and (c) V_{O3} removing O from $O_{(3c)}$ subsurface layer. Isosurfaces (0.005 $e^-/Å^3$) in yellow and blue denote α and β spin densities, respectively, showing that panels a and b correspond to the open-shell singlet state in the unit cell and panel c corresponds to a triplet state. $[TiO_5]$ and $[TiO_4]$ polyhedral are indicated in red and blue, respectively. A dotted circle indicates the position of each V_O. Red and gray spheres represent O and Ti, respectively.

V_{O3} is formed by removing a subsurface $O_{(3c)}$ atom. Two electronic solutions were found for this structure: The most stable, with E_f = 4.61 eV, consists of a partially trapped solution with one reduced $[TiO_4]^{/}$ tetrahedron and two internal $[TiO_5]^{\times}$ polyhedra symmetrically distorted around V_{O3} (Figure 3c). The second configuration, with E_f = 4.78 eV, appears when symmetry around V_{O3} is broken and one $O_{(3c)}$ atom migrates toward the vacancy with a concomitant split fully localized $[TiO_5]^{/}$ + $[TiO_6]^{/}$ electronic solution.

From the preceding discussion, it appears that, for the anatase TiO_2(001) surface, the most stable Vo configuration implies removal of an oxygen atom from the outermost surface atomic layer. This is accompanied by the reduction of two Ti^{4+} cations to Ti^{3+} located at the outermost Ti atomic layer. The corresponding vacancy formation energy of 2.66 eV for this state is in perfect agreement with the 2.98 eV value reported by Ortega et al.[38] and just ~0.2 eV larger than the value calculated by Roldan et al.[10] for the same vacancy position and at the same

DOI: 10.1021/jp5105483
J. Phys. Chem. C 2015, 119, 4805–4816

level of theory (GGA + U with U = 4 eV) but using PW91 instead of PBE as in the present work. It is worth pointing out that a significant difference appears between our PBE results and those reported by Guo et al.[40] They reported a vacancy formation energy of 4.12 eV, in clear disagreement with the much lower 1.29 eV reported here. The origin of the disagreement must be due to the different unit-cell sizes used, implying large differences in defect concentration.

3.3. Oxygen Vacancies in Ce-Doped Anatase TiO_2(001). Different positions for V_O were considered for the Ce-doped anatase TiO_2(001) surface with Ce substituting Ti at either an outermost $Ti_{(5c)}$ or a subsurface $Ti_{(6c)}$ position. Four nonequivalent vacancies near the $[CeO_x]$ polyhedron (corresponding to V_{O1}–V_{O4} in Figure 1) were considered in each case. The standard PBE and PBE(4,4) approaches yielded similar orders of stability of the different V_O sites (Table 3), although the former gave significantly lower E_f values and poor electronic localization, with states with partially delocalized Ce 4f and fully delocalized Ti 3d electrons. For the surface $Ce_{Ti}^{\times}$ substitution, the V_{O1} vacancy is formed by removing one equatorial two-coordinated oxygen from the $[CeO_5]$ polyhedron, resulting in two $[MO_4]$ tetrahedra around the vacancy: $[CeO_5] + [TiO_5] \rightarrow [CeO_4] + [TiO_4] + V_{O1} + 2e + {}^1/_2O_2$. Only the partially localized solution was found for this structure, in which the $[CeO_4]^{/}$ tetrahedron is reduced whereas the other electron is delocalized (Figure 4a). This vacancy is

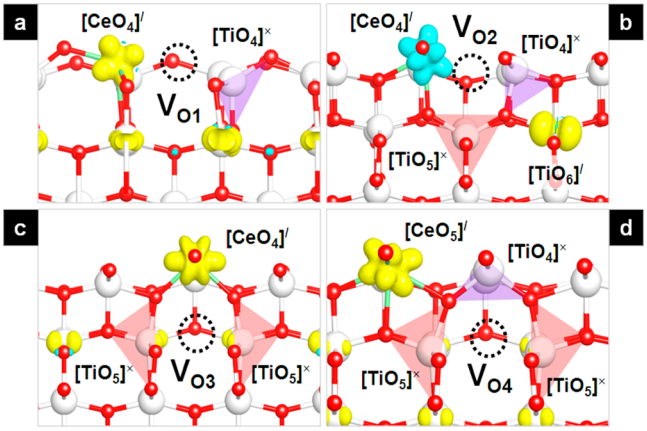

Figure 4. Side views of the structure and spin density isosurfaces (0.005 $e^-/Å^3$) for different vacancy positions around a surface Ce dopant in (001) TiO_2 anatase at the PBE(4,4) level: (a) V_{O1}, (b) V_{O2}, and (c) V_{O3} in the $[CeO_5]$ polyhedron and (d) V_{O4} in the next-neighbor $[TiO_5]$/$[TiO_6]$ polyhedra. Isosurfaces in yellow and blue denote α and β spins, respectively. $[TiO_5]$ and $[TiO_4]$ polyhedra are indicated in red and blue, respectively. A dotted circle indicates the position of the vacancy in each case. Red, gray, and green spheres represent O, Ti, and Ce atoms, respectively.

the most stable when considering the presence of the Ce dopant in the outermost layer of the surface, but with a corresponding E_f value that is larger than for the undoped surface. Again, this disagrees with the decrease in E_f in the presence of a Ce dopant in the outermost layer of anatase (001) reported by Guo et al. (3.73 vs 4.12 eV for the doped and undoped surfaces, respectively).[40] However, they included the +U correction for the Ce 4f states only and compared the resulting value to the (exceedingly large) PBE value for the undoped case, which was already discussed in the previous section of the present work.

The second most stable oxygen vacancy at the PBE(4,4) level around a surface $[CeO_5]$ polyhedron is V_{O2}, formed by removing an external three-fold-coordinated O atom, resulting in three undercoordinated polyhedra: $[CeO_5] + [TiO_5] + [TiO_6] \rightarrow [CeO_4] + [TiO_4] + [TiO_5] + V_{O2} + 2e + {}^1/_2O_2$. At the PBE(4,4) level, only the split localized solution with reduced $[CeO_4]^{/}$ and $[TiO_6]^{/}$ centers in antiferromagnetic coupling was found (Figure 4b). In the presence of a surface Ce atom, the V_{O3} and V_{O4} subsurface vacancies are predicted to be less stable than the V_{O1} and V_{O2} surface-exposed vacancies. The V_{O3} structure, created by removing an apical Ce–O oxygen, results in the configuration $[CeO_5] + 2[TiO_6] \rightarrow [CeO_4] + 2[TiO_5] + V_{O3} + 2e + {}^1/_2O_2$, for which only the partially spin-localized solution was found, in which the $[CeO_4]^{/}$ tetrahedron is reduced (Figure 4c). A similar scenario was found for V_{O4} (Figure 4d) in which the formation of the subsurface vacancy led to the reduction of the exposed $[CeO_5]^{/}$ polyhedron and the delocalization of the other electron, with a resulting value of $E_f(V_{O4})$ = 3.63 eV.

For the Ce-doped anatase TiO_2(001) surface, the most favorable oxygen vacancies are those around a subsurface Ce dopant (Table 3). Among these, V_{O3} is the most stable (Figure 5c). The corresponding electronic state presents several

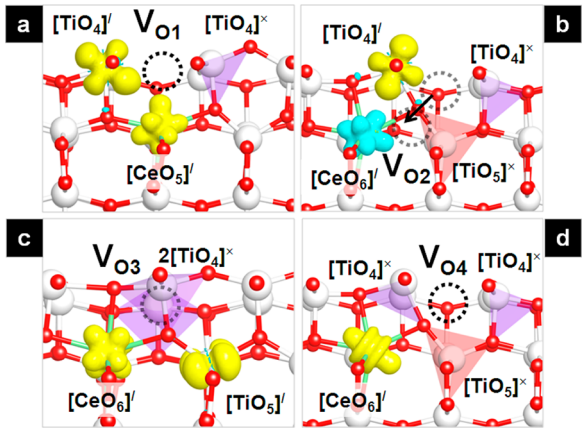

Figure 5. Structure and spin density isosurfaces (0.005 $e^-/Å^3$) for different vacancy positions around a subsurface Ce dopant in (001) TiO_2 anatase at the PBE(4,4) level: (a) V_{O1} and (b) V_{O2} in the $[CeO_5]$ polyhedron (the arrow indicates the migration of $O_{(3c)}$ in the direction of V_{O2} after optimization) and (c) V_{O3} and (d) V_{O4} in the next-neighbor $[TiO_5]$/$[TiO_6]$ polyhedra. Isosurfaces in yellow and blue denote α and β spins, respectively. The polyhedra of $[TiO_5]$ and $[TiO_4]$ in red and blue, respectively. A dotted circle indicates the position of the vacancy in each case. Red, gray, and green spheres represent O, Ti, and Ce atoms, respectively.

stabilizing features leading to a low vacancy formation energy (E_f = 1.82 eV): (i) the vacancy is created by removing one undercoordinated $O_{(2c)}$, which involves breaking only two Ti–O bonds; (ii) full electron trapping forming two reduced subsurface polyhedra ($[CeO_6]^{/}$ + $[TiO_5]^{/}$); and (iii) very pronounced structural distortion, which compensates for the instability of generating a low-coordinated $[TiO_4]^{\times}$ tetrahedron at the surface. These favorable features explain the larger stability of this configuration with respect to all others in either doped or undoped, bulk or surface systems. In addition, for this structure, another electronic state is found with no Ce^{4+}-to-Ce^{3+} reduction but two $[TiO_4]^{/}$ trapped sites. This results in a much larger value of $E_f(V_{O3})$ = 2.43 eV (Table 3), which is

DOI: 10.1021/jp5105483
J. Phys. Chem. C 2015, 119, 4805–4816

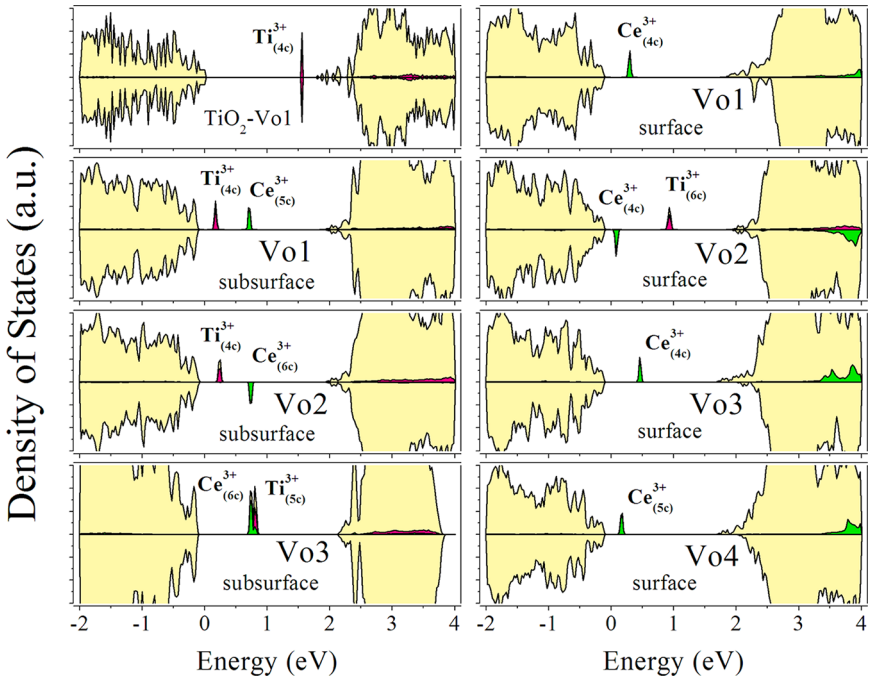

Figure 6. Density of states of selected structures for reduced Ce-doped (a) TiO_2 bulk and (b–h) (001) surfaces at the PBE(4,4) level. The zero energy value has been aligned to the top of the VB (filled O 2p) in each case, whereas the two extra electrons left behind by the removal of a neutral O atom occupying midgap states between the VB and CB correspond to trapped Ti^{3+} $3d^1$ (in red) and Ce^{3+} $4f^1$ (in green) levels.

further evidence of the electron-accepting role of the Ce dopant in Ce-doped titania. The vacancies at the other positions present higher formation energies. Vacancy V_{O4} is the second most stable site associated with subsurface Ce doping with $E_f(V_{O4})$ = 2.75–2.88 eV, which is still lower than for vacancies around a surface $[CeO_5]$ polyhedron. Its structural features are similar to those of V_{O3} in Ce-doped bulk (see Figure 5c in ref 25). The lower energy of this atomic and electronic configuration is also associated with the freedom of the reduced $[CeO_6]^{/}$ octahedron to expand in the (010) plane. The same behavior occurs with two Ce atoms doping in anatase bulk[25] and in the CeO_x/TiO_2 interface.[26] Vacancy V_{O1}, created by removing one apical $O_{(3c)}$ atom bound to the $[CeO_6]$ octahedron, has a corresponding value of $E_f(V_{O1})$ = 3.41 eV, with the two trapped electrons localized at the $[TiO_4]^{/}$ + $[CeO_5]^{/}$ polyhedra (Figure 5a). The calculations involving a vacancy at the V_{O2} position lead to a migration of the oxygen atom shared by the two $[TiO_4]$ tetrahedra toward the $[CeO_5]$ polyhedron, giving rise to the formation of a reduced $[CeO_6]^{/}$ octahedron, E_f = 2.75 eV (Figure 5b), and converging to the V_{O4} structure.

Another aspect regarding the relative stability of the reduced Ce-doped systems must be considered because, when the Ce atom is located at a subsurface position, the E_f values are significantly lower (by ~1.5 eV) than those calculated for the dopant substituting an outermost Ti atom. Nevertheless, the substitution at the outermost position is more than 2 eV more favorable than the substitution at a subsurface position. These energy differences have the same origin, which is the instability of the (001) surface: Distorting the outermost surface layer with a Ce dopant has a larger compensating effect than having Ce at a subsurface position. Furthermore, when the surface has already been largely stabilized by doping at the outermost layer, generating an oxygen vacancy is more difficult, and this is why calculated vacancy formation energies are lower when Ce is at a subsurface position. Because the compensating effect of Ce is larger than that of reduction, the most stable structure for reduced Ce-doped (001) anatase corresponds to that with the Ce atom at the outermost surface layer from which an undercoordinated $O_{(2c)}$ atom has been removed, although the associated vacancy formation energy for this state is not among the lowest calculated values. Therefore, the presence of Ce is considered to benefit the formation of O vacancies, but only when the dopant Ce atom is located at subsurface positions, which is not the most stable case.

3.4. Effect of Ce Doping in the Electronic Structure of Reduced TiO_2 Anatase (001). The total and projected DOS for selected stoichiometric and Ce-doped anatase TiO_2(001) surface states are shown in Figure 6.

The DOS features of the reduced TiO_2 surfaces (Figure 6a) are qualitatively similar to those of the reduced bulk TiO_2 and Ce-doped TiO_2 bulk systems reported in a previous work.[25] The two electrons left upon V_O formation occupy midgap states, lying between 0.5 and 1 eV below the bottom of the conduction band (CB). However, the exact position of the midgap states depends on the environment of the oxygen vacancy. For the subsurface-$[CeO_6]$-doped system, the fully trapped solution led to a Ti $3d^1$ state at lower energies than the Ce $4f^1$ state for V_{O1} and V_{O2} (panels b and c, respectively, of Figure 6), whereas for the more stable V_{O3} (Figure 6d), the midgap states were almost degenerate. The greater stability of the reduced structure leading to degenerate midgap states was also found for vacancies in the Ce-doped bulk anatase.[25] These similarities are not surprising because subsurface vacancies closely resemble those in the bulk, involving the reduction of similarly coordinated $[CeO_6]$ polyhedra. On the other hand, for the surface-Ce-doped systems, the midgap Ce^{3+} 4f states always lie at lower energies than the Ti^{3+} 3d levels (Figure 6e–h), the latter usually being delocalized and thus not leading to the narrow midgap states of other systems. These differences arise

DOI: 10.1021/jp5105483
J. Phys. Chem. C 2015, 119, 4805–4816

from the different positions of the unoccupied Ce 4f states for the different systems mentioned earlier and represented in Figure 3. Thus, larger (smaller) overlap of the unoccupied Ti 3d and Ce 4f bands in the unreduced systems leads to more (fewer) degenerate midgap states when oxygen vacancies are formed. It should be noted that other solutions with different electron trapping can be found differing mainly in the Ti atom that is reduced, which can change the depth of midgap states. However, we found the fully localized solution in the most stable vacancy associated with cerium doped in both the bulk and the (001) surface, which indicates that states with fully localized electrons (midgap states) are more stable. The Bader charges were also calculated for the different metal atoms within the systems studied. For the stoichiometric systems, the calculated Bader charges were far from the formal charge values, as expected for oxides with a certain degree of covalent character such as TiO_2 or CeO_2. Therefore, Ti^{4+} and Ce^{4+} species feature characteristic Bader charges of ~2.3 *e* and ~2.4 *e*, respectively. In addition, when one of the electrons left behind by the removed O atoms occupies either a Ti 3d or a Ce 4f orbital, the Bader charges are reduced by ~0.2 *e* for the cation accepting the electron.

Figure 7 contains a graphical summary of the effect of Ce doping on the oxygen vacancy formation energy (E_f) for the

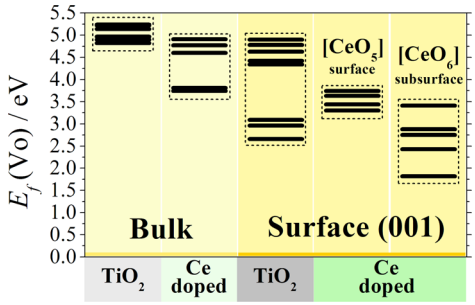

Figure 7. Oxygen vacancy formation energies at the PBE+(4,4) level for the different systems considered in this work and in ref 25, showing that V_O occurs more favorably in Ce-doped than in TiO_2 anatase in both the bulk and surface phases and can be enhanced by subsurface doping instead substitution in the outmost [TiO_5] layer. The most stable configurations within reduced Ce-doped systems are associated with the reduction of Ce^{4+} to Ce^{3+}.

different systems taken into consideration and of the differences between the bulk and the (001) surface. The undercoordinated O atoms in the outermost layer of the (001) surface are more weakly bound than those in the bulk, leading to lower vacancy formation energies. In addition, the presence of the dopant in the bulk reduces E_f by ~1.2 eV as a result of the lower energy of the Ce 4f bands that accept one of the electrons coming from the removed O atom. A similar effect occurs when the Ce atom is in a subsurface site. In this case, E_f is greatly reduced because of the combination of two effects; removal of weakly bound $O_{(2c)}$ atoms is further facilitated by the possibility of reducing Ce^{4+} ($4f^0$) to Ce^{3+} ($4f^1$). However, the same behavior is not detected when the Ce atom is substituting a Ti atom at the outermost layer of the surface. This is due to the large stability of the surface complex formed upon such substitution; removing an O atom from such a stable moiety results in higher vacancy formation energies than in the absence of the Ce atom.

3.5. Ab Initio Thermodynamic Analysis. To evaluate the stability of the different systems considered under different conditions, we carried out an ab initio thermodynamic analysis.[66,67] For the ab initio thermodynamic analysis, we assumed that (i) only oxygen vacancies (V_O) and Ce dopant are present as point defects in the bulk and surfaces; (ii) all entropic and vibrational contributions are neglected for the solid phase; (iii) the Gibbs free energy can be approximated by the total DFT energy; and (iv) metal oxides are in thermodynamic equilibrium with Ti, Ce, and oxygen during growth. Because we considered only one kind of Ce doping ($Ce_{Ti}^{\times}$) in two possible sites ($Ti_{(6c)}$ and $Ti_{(5c)}$), the Ce and Ti reference were their bulk oxides, TiO_2 and CeO_2, instead of the chemical potentials of isolated atoms or bulk metal. As shown in our previous work,[25] using the oxides as references for calculating the substitution/doping energy provides more suitable results. The general equation for Ce-for-Ti substitution in the 3 × 3 × 1 supercell is then expressed as

$$Ti_{36}O_{72} + xCeO_2 \rightarrow Ti_{36-x}Ce_xO_2 + xTiO_2$$

To construct a (T, p) diagram of surface-defective systems, we can include the variation of the oxygen chemical potential $\Delta\mu_O$ in eq 3. For any system, the total surface free energy, herein referred to as γ_f (meV A^{-2}), can be expressed as the sum of the cerium doping energy and the vacancy formation energy

$$\Delta\gamma_f = \left(\frac{1}{2A}\right)\{E_{slab}^{DFT}(Ti_{36-x}Ce_xO_{72-y}) - E_{slab}^{DFT}(Ti_{36}O_{72}) - y[\Delta\mu_O(T,p)]\} + x[E_{bulk}^{DFT}(TiO_2) - E_{bulk}^{DFT}(CeO_2)] \quad (4)$$

where the change in the oxygen chemical potential is expressed as one-half of the total DFT energy of the O_2 molecule in its triplet ground state, which can, in turn, be expressed as a function of temperature T and oxygen partial pressure $p(O_2)$

$$\Delta\mu_O(T,p) = \mu_O(T,p) - \frac{1}{2}E_{(O_2)}^{DFT} = \mu_O(T,p^\circ) + \frac{1}{2}kT\ln(p/p^\circ) - \frac{1}{2}E_{(O_2)}^{DFT} \quad (5)$$

After some algebraic manipulation, we derive the expressions

$$E_f(V_O) = \left(\frac{1}{2A}\right)\{E_{slab}^{DFT}(Ti_{36}O_{72-y}) - E_{slab}^{DFT}(Ti_{36}O_{72}) - y[\Delta\mu_O(T,p)]\} \quad (6)$$

$$\Delta\gamma_f = \left(\frac{1}{2A}\right)\{E_{slab}^{DFT}(Ti_{36-x}Ce_xO_{72-y}) - E_{slab}^{DFT}(Ti_{36-x}Ce_xO_{72}) - y[\Delta\mu_O(T,p)]\} \quad (7)$$

for the Gibbs formation energy, in which the vacancy formation energy $E_f(V_O)$ as calculated according to eq 3 emerges naturally when T = 0. The standard chemical potential at several temperatures can be taken from ref 66.

The O-rich limit for the oxygen chemical potential corresponds to the value at which oxygen molecules start to condense, $\Delta\mu_O$ = 0. The O-poor limit corresponds to the oxygen chemical potential at which metal particles begin to crystallize, $\mu_{Ti} = E_{Ti}$ and $\mu_{Ce} = E_{Ce}$, where E_{Ti} and E_{Ce} are the total DFT energies of Ti and Ce ground-state bulk metals, respectively. Using the condition of equilibrium $E_{MO_2} - E_M < \Delta\mu_O$, where E_{MO_2} is the bulk formation energy of the oxide

DOI: 10.1021/jp5105483
J. Phys. Chem. C 2015, 119, 4805−4816

MO_2 (computed as 9.4 eV for TiO_2 anatase, compared to an experimental value of 9.8 eV,[68] and 10.5 eV for CeO_2 fluorite, compared to an experimental value of 10.62 eV[69]), we obtain the following O-rich/O-poor ranges: -4.6 eV $< \Delta\mu_O < 0$ for TiO_2 and -6.2 eV $< \Delta\mu_O < 0$ for CeO_2.

The evolution of the surface free energy (eq 7) (hereafter referred to simply as the surface energy, for simplicity) as a function of the chemical potential μ_O is presented in Figure 8.

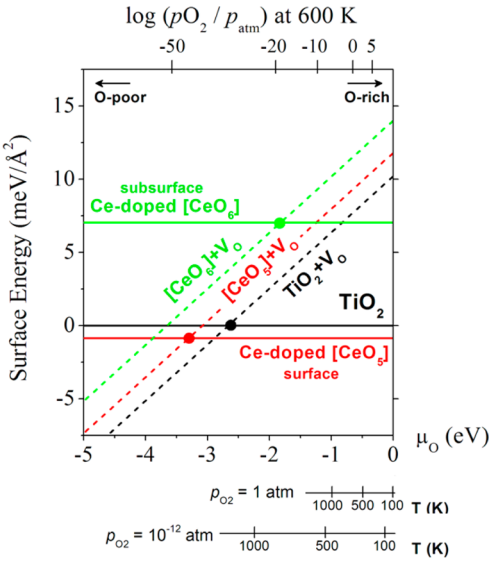

Figure 8. Evolution of the surface energy (meV/Å) at the PBE + U level of the different systems as a function of the oxygen chemical potential. The partial pressure scale at 600K and temperature scales at two constant values of the partial pressure corresponding to ultrahigh-vacuum (UHV) conditions (10^{-12} atm) and to atmospheric pressure (1 atm) are also shown.

Because the chemical potential depends on T and p, the x axis can be conveniently transformed into a temperature scale at constant pressure (or vice versa). Thus, in addition to the chemical potential, we include the equivalent temperature scale at two constant values of the partial pressure corresponding to ultrahigh-vacuum (UHV) conditions (10^{-12} atm) and to atmospheric pressure (1 atm). Using these two representative pressure regimes allows the different behaviors between experiments performed at UHV and standard conditions to be assessed. In particular, we found that, whereas the formation of oxygen vacancies for undoped TiO_2(001) would begin above 1000 K under UHV conditions, a much higher temperature would be needed to start generating vacancies at atmospheric pressure, exceeding the phase transition from anatase to rutile (~900 K).[70] For the Ce-doped cases, as expected from the oxygen vacancy formation energies for these systems, these points are shifted toward higher or lower temperatures depending on whether the Ce atom occupies surface or subsurface positions, respectively. Nevertheless, although vacancies around a subsurface Ce dopant would form at lower temperatures, the states with Ce at the subsurface are less favorable than those with a Ce dopant at the outermost surface layer of TiO_2(001), as indicated by the Ce-subsurface states lying at lower energies. Furthermore, the lower temperatures (energies) required to form vacancies for undoped TiO_2(001) than for the most stable Ce-doped case indicate that, for the unreconstructed TiO_2(001) surface, it is preferable to have O vacancies away from Ce substituents.

4. CONCLUSIONS

The effects of Ce doping on the electronic properties and reducibility of the TiO_2 anatase (001) surface were studied by means of periodic DFT calculations within both the standard PBE and the partially corrected PBE + U approaches. The natures of reduced Ce^{3+} and Ti^{3+} centers were investigated for different dopant and oxygen vacancy positions at the surface. For undoped anatase TiO_2(001), various solutions involving reduced Ti^{3+} species at surface and subsurface positions were obtained with different electronic structures (including simple, split, and partial localization of the unpaired electrons of the system). Fully delocalized solutions were obtained whenever the electronic self-interaction error was not sufficiently corrected. In addition, the localized states obtained at the PBE + U level were found to occupy midgap levels lying 0.50–1.00 eV below the CB. For the undoped surface, the most stable vacancy site was found to correspond to the removal of an undercoordinated outermost surface $O_{(2c)}$ atom.

The presence of the Ce dopant at the surface or subsurface was found to lead to a significant decrease in the surface energy and a slight decrease in the band gap through the introduction empty Ce $4f^0$ states below the conduction band of anatase. These effects were more pronounced when the Ce atom was at the outermost position, which is the most stable location for this dopant, indicating that the migration of the dopant to the surface is thermodynamically favorable. With respect to vacancy formation, both PBE and PBE + U calculations consistently predicted that, whereas the formation of oxygen vacancies is favored by the presence of the dopant at a subsurface position, the great stability of the surface complex formed upon doping at an outermost surface position leads to larger vacancy formation energies than for the undoped case. As a result, for the unreconstructed TiO_2(001) surface, it is more favorable to have O vacancies away from Ce substituents. In addition, for all surfaces, the most easily removable O atom corresponds to an outermost two-fold-coordinated oxygen $O_{(2c)}$ atom, and its removal leads to the reduction of one Ti^{4+} ion to Ti^{3+} and of one Ce^{4+} ion to Ce^{3+}, as indicated by the spin density featuring unpaired electrons on these cations and their reduced Bader charges. Different vacancy positions lead to varying positions of the occupied midgap levels, whose existence leads to the formation of channels for visible light absorption.

Generally, the reducibility (stability of vacancies) of the studied systems can be ordered as follows: Ce-subsurface-TiO_2(001) > TiO_2(001) > Ce-surface-TiO_2(001) > Ce-bulk-TiO_2 > bulk-TiO_2.

AUTHOR INFORMATION

Corresponding Author

*Tel.: +34 934 021 229. Fax: +34 934 021 231. E-mail: francesc.illas@ub.edu.

Notes

The authors declare no competing financial interest.

ACKNOWLEDGMENTS

This work was supported by Brazilian Funding Agencies FAPESP, CNPq, and INCTMN-Unesp; a Spanish MINECO CTQ2012-30751 grant; and, in part, by Generalitat de Catalunya Grants 2014GR97 and XRQTC. A.R.A. thanks the Brazilian scholarship program "Ciência sem Fronteiras" (Process 237539/2012-8). The authors acknowledge computer facilities supported by the Consorci de Serveis Universitaris de

DOI: 10.1021/jp5105483
J. Phys. Chem. C 2015, 119, 4805–4816

Catalunya (CSUC; formerly CESCA). F.I. acknowledges additional financial support through a 2009 ICREA Academia Award for Excellence in University Research. We acknowledge financial support from the EU (COST Action CM1104).

REFERENCES

(1) Fujishima, A.; Zhang, X.; Tryk, D. TiO_2 Photocatalysis and Related Surface Phenomena. *Surf. Sci. Rep.* **2008**, *63*, 515−582.
(2) Chen, H.; Nanayakkara, C. E.; Grassian, V. H. Titanium Dioxide Photocatalysis in Atmospheric Chemistry. *Chem. Rev.* **2012**, *112*, 5919−5948.
(3) Yang, H. G.; Sun, C. H.; Qiao, S. Z.; Zou, J.; Liu, G.; Smith, S. C.; Cheng, H. M.; Lu, G. Q. Anatase TiO_2 Single Crystals with a Large Percentage of Reactive Facets. *Nature* **2008**, *453*, 638−641.
(4) Kavan, L.; Grätzel, M.; Gilbert, S. E.; Klemenz, C.; Scheel, H. J. Electrochemical and Photoelectrochemical Investigation of Single-Crystal Anatase. *J. Am. Chem. Soc.* **1996**, *118*, 6716.
(5) Sanjines, R.; Tang, H.; Berger, H.; Gozzo, F.; Margaritondo, G.; Levy, F. Electronic structure of anatase TiO2 oxide. *J. Appl. Phys.* **1994**, *75*, 2945−2951.
(6) Miao, L.; Tanemura, S.; Kaneko, K.; Terai, A.; Nabatova-Gabain, N. Simultaneous sputter growth of epitaxial anatase and rutile TiO_2 thin films with high refractive índex. *J. Cryst. Growth* **2003**, *254*, 100−106.
(7) Chen, X.; Liu, L.; Yu, P. Y.; Mao, S. S. Increasing Solar Absorption for Photocatalysis with Black Hydrogenated Titanium Dioxide Nanocrystals. *Science* **2011**, *331*, 746−750.
(8) Wu, Q.; Liu, M.; Wu, Z.; Li, Y.; Piao, L. Is Photooxidation Activity of {001} Facets Truly Lower Than That of {101} Facets for Anatase TiO_2 Crystals? *J. Phys. Chem. C* **2012**, *116*, 26800−26804.
(9) Tosoni, S.; Lamiel-Garcia, O.; Hevia, D. F.; Doña, J. M.; Illas, F. Electronic Structure of F-Doped Bulk Rutile, Anatase, and Brookite Polymorphs of TiO_2. *J. Phys. Chem. C* **2012**, *116*, 12738−12746.
(10) Roldán, A.; Boronat, M.; Corma, A.; Illas, F. Theoretical Confirmation of the Enhanced Facility to Increase Oxygen Vacancy Concentration in TiO_2 by Iron Doping. *J. Phys. Chem. C* **2010**, *114*, 6511−6517.
(11) Petrik, N. G.; Zhang, Z.; Du, Y.; Dohnálek, Z.; Lyubinetsky, I.; Kimmel, G. A. Chemical Reactivity of Reduced TiO_2(110): The Dominant Role of Surface Defects in Oxygen Chemisorption. *J. Phys. Chem. C* **2009**, *113*, 12407−12411.
(12) Watanabe, S.; Ma, X.; Song, C. Characterization of Structural and Surface Properties of Nanocrystalline TiO_2−CeO_2 Mixed Oxides by XRD, XPS, TPR, and TPD. *J. Phys. Chem. C* **2009**, *113*, 14249−14257.
(13) Park, J. B.; Graciani, J.; Evans, J.; Stacchiola, D.; Senanayake, S. D.; Barrio, L.; Liu, P.; Fdez. Sanz, J.; Hrbek, J.; Rodriguez, J. A. Gold, Copper, and Platinum Nanoparticles Dispersed on CeOx/TiO_2(110) Surfaces: High Water-Gas Shift Activity and the Nature of the Mixed-Metal Oxide at the Nanometer Level. *J. Am. Chem. Soc.* **2010**, *132*, 356−363.
(14) Bruix, A.; Rodriguez, J. A.; Ramírez, P. J.; Senanayake, S. D.; Evans, J.; Park, J. B.; Stacchiola, D.; Liu, P.; Hrbek, J.; Illas, F. A New Type of Strong Metal−Support Interaction and the Production of H_2 Through the Transformation of Water on Pt/CeO_2(111) and Pt/CeOx/TiO_2(110) Catalysts. *J. Am. Chem. Soc.* **2012**, *134*, 8968−8974.
(15) Carrettin, S.; Hao, Y.; Aguilar-Guerrero, V.; Gates, B. C.; Trasobares, S.; Calvino, J. J.; Corma, A. Increasing the Number of Oxygen Vacancies on TiO_2 by Doping with Iron Increases the Activity of Supported Gold for CO Oxidation. *Chem.—Eur. J.* **2007**, *13*, 7771−7779.
(16) Carrettin, S.; Mc Morn, P.; Johnston, P.; Griffin, K.; Kiely, C. J.; Hutchings, G. J. Oxidation of Glycerol Using Supported Pt, Pd and Au Catalysts. *Phys. Chem. Chem. Phys.* **2003**, *5*, 1329−1336.
(17) Nolan, M. Charge Compensation and Ce^{3+} Formation in Trivalent Doping of the CeO_2(110) Surface: The Key Role of Dopant Ionic Radius. *J. Phys. Chem. C* **2011**, *115*, 6671−6681.
(18) Zhang, Y.; Lv, F.; Wu, T.; Yu, L.; Zhang, R.; Shen, Bo.; Meng, X.; Ye, Z.; Chu, P. K. F and Fe Co-Doped TiO_2 with Enhanced Visible Light Photocatalytic Activity. *J. Sol-Gel Sci. Technol.* **2011**, *59*, 387−391.
(19) Farra, R.; García-Melchor, M.; Eichelbaum, M.; Hashagen, M.; Frandsen, W.; Allan, J.; Girgsdies, F.; Szentmiklósi, L.; López, N.; Teschner, D. Promoted Ceria: A Structural, Catalytic, and Computational Study. *ACS Catal.* **2013**, *3*, 2256−2268.
(20) Choudhury, B.; Borah, B.; Choudhury, A. Extending Photocatalytic Activity of TiO_2 Nanoparticles to Visible Region of Illumination by Doping of Cerium. *Photochem. Photobiol.* **2012**, *88*, 257−264.
(21) Chen, S. W.; Lee, J. M.; Lu, K. T.; Pao, C. W.; Lee, J. F.; Chan, T. S.; Chen, J. M. Band-Gap Narrowing of TiO_2 Doped with Ce Probed with X-ray Absorption Spectroscopy. *Appl. Phys. Lett.* **2010**, *97*, 012104.
(22) Liu, T. X.; Li, X. Z.; Li, F. B. Enhanced photocatalytic activity of Ce^{3+}-TiO_2 hydrosols in aqueous and gaseous phases. *Chem. Eng. J.* **2010**, *157*, 475−482.
(23) Li, F. B.; Li, X. Z.; Hou, M. F.; Cheah, K. W.; Choy, W. C. H. Enhanced photocatalytic activity of Ce^{3+}−TiO_2 for 2-mercaptobenzothiazole degradation in aqueous suspension for odour control. *Appl. Catal. A: Gen.* **2005**, *285*, 181−189.
(24) Tong, T.; Zhang, J.; Tian, B.; Chen, F.; He, D.; Anpo, M. Preparation of Ce−TiO_2 catalysts by controlled hydrolysis of titanium alkoxide based on esterification reaction and study on its photocatalytic activity. *J. Colloid Interface Sci.* **2007**, *315*, 382−388.
(25) Albuquerque, A. R.; Bruix, A.; Santos, I. M. G.; Sambrano, J.; Illas, F. A DFT Study on Ce-Doped Anatase TiO_2: Nature of Ce^{3+} and Ti^{3+} Centers Triggered by Oxygen Vacancy Formation. *J. Phys. Chem. C* **2014**, *118*, 9677−9689.
(26) Johnston-Peck, A. C.; Senanayake, S. D.; Plata, J. J.; Kundu, S.; Xu, W.; Barrio, L.; Graciani, J.; Fdez. Sanz, J.; Navarro, R. M.; Fierro, J. L. G.; Stach, E. A.; Rodriguez, J. A. Nature of the Mixed-Oxide Interface in Ceria−Titania Catalysts: Clusters, Chains, and Nanoparticles. *J. Phys. Chem. C* **2013**, *117*, 14463−14471.
(27) Liu, G.; Yang, H. G.; Pan, J.; Yang, Y. Q.; Lu, G. Q. (Max); Cheng, H. M. Titanium Dioxide Crystals with Tailored Facets. *Chem. Rev.* **2014**, *114*, 9559−9612.
(28) Zhang, J.; Chen, S.; Qian, L.; Tao, X.; Yang, L.; Wang, H.; Li, Y.; Zhang, E.; Xi, J.; Ji, Z. Regulating Photocatalytic Selectivity of Anatase TiO_2 with {101}, {001}, and {111} Facets. *J. Am. Ceram. Soc.* **2014**, *97*, 4005−4010.
(29) Auer, S.; Frenkel, D. Suppression of Crystal Nucleation in Polydisperse Colloids due to Increase of the Surface Free Energy. *Nature.* **2001**, *413*, 711−713.
(30) Xing, M.-Y.; Yang, B.-X.; Yu, H.; Tian, B.-Z.; Bagwasi, S.; Zhang, J.-L.; Gong, X.-Q. Enhanced Photocatalysis by Au Nanoparticle Loading on TiO_2 Single-Crystal (001) and (110) Facets. *J. Phys. Chem. Lett.* **2013**, *4*, 3910−3917.
(31) Ichimura, A. S.; Mack, B. M.; Usmani, S. M.; Mars, D. G. Direct Synthesis of Anatase Films with 100% (001) Facets and [001] Preferred Orientation. *Chem. Mater.* **2012**, *24*, 2324−2329.
(32) Miao, J.; Liu, B. Anatase TiO_2 microspheres with reactive {001} facets for improved photocatalytic activity. *RSC Adv.* **2013**, *3*, 1222−1226.
(33) Yang, X. H.; Li, Z.; Sun, C.; Yang, H. G.; Li, C. Hydrothermal Stability of {001} Faceted Anatase TiO_2. *Chem. Mater.* **2011**, *23*, 3486−3494.
(34) Setvín, M.; Aschauer, U.; Scheiber, P.; Li, Y.-F.; Hou, W.; Schmid, M.; Selloni, A.; Diebold, U. Reaction of O_2 with Subsurface Oxygen Vacancies on TiO_2 Anatase (101). *Science.* **2013**, *341*, 988−991.
(35) Cheng, H.; Selloni, A. Surface and Subsurface Oxygen Vacancies in Anatase TiO_2 and Differences with Rutile. *Phys. Rev. B* **2009**, *79*, 092101.
(36) Setvin, M.; Aschauer, U.; Scheiber, P.; Li, Y. F.; Hou, W. Y.; Schmid, M.; Selloni, A.; Diebold, U. Reaction of O_2 with Subsurface

DOI: 10.1021/jp5105483
J. Phys. Chem. C 2015, 119, 4805−4816

Oxygen Vacancies on TiO_2 Anatase (101). *Science* **2013**, *341*, 988−991.
(37) Scheiber, P.; Fidler, M.; Dulub, O.; Schmid, M.; Diebold, U.; Hou, W. Y.; Aschauer, U.; Selloni, A. (Sub)Surface Mobility of Oxygen Vacancies at the TiO_2 Anatase (101) Surface. *Phys. Rev. Lett.* **2012**, *109*, 136103.
(38) Ortega, Y.; Hevia, D. F.; Oviedo, J.; San-Miguel, M. A. A DFT study of the stoichiometric and reduced anatase (001) surfaces. *Appl. Surf. Sci.* **2014**, *294*, 42−48.
(39) Yamamoto, T.; Ohno, T. A Hybrid Density Functional Study on the Electron and Hole Trap States in Anatase Titanium Dioxide. *Phys. Chem. Chem. Phys.* **2012**, *14*, 589−598.
(40) Guo, J.; Janik, M. J.; Song, C. Density Functional Theory Study on the Role of Ceria Addition in $Ti_xCe_{1-x}O_2$ Adsorbents for Thiophene Adsorption. *J. Phys. Chem. C* **2012**, *116*, 3457−3466.
(41) Kotomin, E. A.; Alexandrov, V.; Gryaznov, D.; Evarestov, R. A.; Maier, J. Confinement effects for ionic carriers in $SrTiO_3$ ultrathin films: first-principles calculations of oxygen vacancies. *Phys. Chem. Chem. Phys.* **2011**, *13*, 923−926.
(42) Hengerer, R.; Bollinger, B.; Erbudak, M.; Grätzel, M. Structure and stability of the anatase TiO_2 (101) and (001) surfaces. *Surf. Sci.* **2000**, *460*, 162−169.
(43) Wang, Y.; Sun, H.; Tan, S.; Feng, H.; Cheng, Z.; Zhao, J.; Zhao, A.; Wang, B.; Luo, Y.; Yang, J.; Hou, J. G. Role of Point Defects on the Reactivity of Reconstructed Anatase Titanium Dioxide (001) Surface. *Nat. Commun.* **2013**, *4*, 2214.
(44) Finazzi, E.; Valentin, C. D.; Pacchioni, G.; Selloni, A. Excess Electron States in Reduced Bulk Anatase TiO_2: Comparison of Standard GGA, GGA + *U*, and Hybrid DFT Calculations. *J. Chem. Phys.* **2008**, *129*, 154113−154119.
(45) Kresse, G.; Hafner, J. Ab Initio Molecular Dynamics for Liquid Metals. *Phys. Rev. B* **1993**, *47*, 558−561.
(46) Kresse, G.; Furthmüller, J. Efficient Iterative Schemes for ab Initio Total-Energy Calculations Using a Plane-Wave Basis Set. *Phys. Rev. B* **1996**, *54*, 11169−11186.
(47) Perdew, J. P.; Burke, K.; Ernzerhof, M. Generalized Gradient Approximation Made Simple. *Phys. Rev. Lett.* **1996**, *77*, 3865−3868.
(48) Blöchl, P. E. Projector Augmented-Wave Method. *Phys. Rev. B* **1994**, *50*, 17953−17979.
(49) Anisimov, V. I.; Zaanen, J.; Andersen, O. K. Band Theory and Mott Insulators: Hubbard *U* Instead of Stoner *I*. *Phys. Rev. B* **1991**, *44*, 943−954.
(50) Liechtenstein, A. I.; Anisimov, V. I.; Zaanen, J. Density-functional theory and strong interactions: Orbital ordering in Mott−Hubbard insulators. *Phys. Rev. B* **1995**, *52*, 5467−5470.
(51) Dudarev, S. L.; Botton, G. A.; Savrasov, S. Y.; Humphreys, C. J.; Sutton, A. P. Electron-energy-loss spectra and the structural stability of nickel oxide: An LSDA+U study. *Phys. Rev. B* **1998**, *57*, 1505−1509.
(52) Ganduglia-Pirovano, M. V.; Da Silva, J. L. F.; Sauer, J. Density-Functional Calculations of the Structure of Near-Surface Oxygen Vacancies and Electron Localization on CeO_2(111). *Phys. Rev. Lett.* **2009**, *102*, 26101−26104.
(53) Pople, J. A.; Head-Gordon, M.; Fox, D. J.; Raghavachar, K.; Curtiss, L. A. Gaussian-1 theory: A general procedure for prediction of molecular energies. *J. Chem. Phys.* **1989**, *90*, 5622.
(54) Horn, M.; Schwerdt, C. F.; Meagher, E. P. Refinement of Structure of Anatase at Several Temperatures. *Z. Kristallogr.* **1972**, *136*, 273−281.
(55) Ortega, Y.; Lamiel-Garcia, O.; Hevia, D. F.; Tosoni, S.; Oviedo, J.; San-Miguel, M. A.; Illas, F. Theoretical study of the fluorine doped anatase surfaces. *Surf. Sci.* **2013**, *618*, 154−158.
(56) Mino, L.; Ferrari, A. M.; Lacivita, V.; Spoto, G.; Bordiga, S.; Zecchina, A. CO Adsorption on Anatase Nanocrystals: A Combined Experimental and Periodic DFT Study. *J. Phys. Chem. C* **2011**, *115*, 7694−7700.
(57) Wulff, G. On the question of the rate of growth and dissolution of crystal surfaces. *Z. Kristallogr. Miner.* **1901**, *34*, 449−530.
(58) Bromley, S. T.; de P. R. Moreira, I.; Neyman, K. M.; Illas, F. Approaching nanoscale oxides: Models and theoretical methods. *Chem. Soc. Rev.* **2009**, *38*, 2657−2670.
(59) Tang, H.; Lévy, F.; Berger, H.; Schmid, P. E. Urbach Tail of Anatase TiO_2. *Phys. Rev. B* **1995**, *52*, 7771−7774.
(60) Vu, N. H.; Le, H. V.; Cao, T. M.; Pham, V. V.; Le, H. M.; Nguyen-Manh, D. Anatase−Rutile Phase Transformation of Titanium Dioxide Bulk Material: A DFT + *U* Approach. *J. Phys.: Condens. Matter* **2012**, *24*, 405501−405511.
(61) Morgan, B. J.; Watson, G. W. A DFT + *U* Description of Oxygen Vacancies at the TiO_2 Rutile (110) Surface. *Surf. Sci.* **2007**, *601*, 5034−5041.
(62) Tosoni, S.; Fernandez Hevia, D.; González Díaz, O.; Illas, F. Origin of Optical Excitations in Fluorine-Doped Titania from Response Function Theory: Relevance to Photocatalysis. *J. Phys. Chem. Lett.* **2012**, *3*, 2269.
(63) Gionco, C.; Paganini, M. C.; Giamello, E.; Burgess, R.; Di Valentin, C.; Pacchioni, G. Cerium-Doped Zirconium Dioxide, a Visible-Light-Sensitive Photoactive Material of Third Generation. *J. Phys. Chem. Lett.* **2014**, *5*, 447−451.
(64) Aschauer, U.; He, Y.; Cheng, H.; Li, S.; Diebold, U.; Selloni, A. Influence of Subsurface Defects on the Surface Reactivity of TiO_2: Water on Anatase (101). *J. Phys. Chem. C* **2010**, *114*, 1278−1284.
(65) Gong, X.; Selloni, A.; Dulub, O.; Jacobson, P.; Diebold, U. Small Au and Pt Clusters at the Anatase TiO_2(101) Surface: Behavior at Terraces, Steps, and Surface Oxygen Vacancies. *J. Am. Chem. Soc.* **2008**, *130*, 370−381.
(66) Reuter, K.; Scheffler, M. Composition, structure, and stability of RuO_2(110) as a function of oxygen pressure. *Phys. Rev. B* **2001**, *65*, 035406.
(67) Prada, S.; Giordano, L.; Pacchioni, G. Charging of Gold Atoms on Doped MgO and CaO: Identifying the Key Parameters by DFT Calculations. *J. Phys. Chem. C* **2013**, *117*, 9943−9951.
(68) Lide, D. R., Ed. *CRC Handbook of Chemistry and Physics*; CRC Press: Boca Raton, FL, 2000.
(69) Trovarelli, A. *Catalysis by Ceria and Related Materials*; World Scientific Publishing Company: Singapore, 2002.
(70) Hanaor, D. A. H.; Sorrell, C. C. Review of the anatase to rutile phase transformation. *J. Mater. Sci.* **2011**, *46*, 855−874.

DOI: 10.1021/jp5105483
J. Phys. Chem. C 2015, 119, 4805−4816